Non-mechanically-axial-scanning confocal microscope using adaptive mirror switching

Yoshiaki Yasuno, Shuichi Makita and Toyohiko Yatagai

Institute of Applied Physics, University of Tsukuba, Tennôdai 1-1-1, Tsukuba, Ibaraki, 305-8573, Japan

yasuno@optlab2.bk.tsukuba.ac.jp

http://optics.bk.tsukuba.ac.jp/COG/

Tobias F. Wiesendanger, Aiko K. Ruprecht and Hans J. Tiziani

Institut für Technische Optik, Universität Stuttgart, Pfaffenwaldring 9, 70569 Stuttgart, Germany

http://www.uni-stuttgart.de/ito/

Abstract: A non-axial-scanning confocal microscope employing a monochromatic light source has been developed. The system controls the defocus of an objective into three to five optimized states by using a membrane-adaptive mirror, and determines the axial height of an object according to the confocal output value with each defocus. A genetic algorithm is employed to optimize the adaptive mirror shape, with the information entropy of the spectrum of the lateral confocal spot profile used as a cost function in the genetic algorithm. Our experimental system successfully determined axial object height within 50 μm range with 0.64 % of error.

OCIS codes: (180.1790) Confocal microscopy; (120.2830) Height measurements

References and links

1. Jordan M. and Wegner M. and Tiziani H. J., "Highly accurate non-contact characterization of engineering surfaces using confocal microscoy," Measurement Sci. Technol. **9**, 1142–1151 (1998).
2. D. T. Fewer and S. J. Hewlett and E. M. McCabe, "Laser Sources in Direct-View-Scanning, Tandem-Scanning, or Nipkow-Disk-Scanning Confocal Microscopy," Appl. Opt. **37**, 380–385 (1998).
3. S. Yin and G. Lu and J. Zhang and F. T. S. Yu and Joseph N. Mait, "Kinoform-based Nipkow disk for a confocal microscope," Appl. Opt. **34**, 5695–5698 (1995).
4. Hans J. Tiziani and Hans-Martin Uhde, "Three-dimensional analysis by a microlens-array confocal arrangement," Appl. Opt. **33**, 567–572 (1994).
5. Tiziani H. J. and Achi R. and Krämer R. N. and Hessler T. and Gale M. T. and Rossi M. and Kunz R. E., "Microlens arrays for confocal microscopy," Opt. Laser Tech. **29**, 85–91 (1997).
6. T. Tanaami and S. Otsuki and N. Tomosada and Y. Kosugi and M. Shimizu and H. Ishida, "High-Speed 1-Frame /ms Scanning Confocal Microscope with a Microlens and Nipkow Disks," Appl. Opt. **41**, 4704–4708 (2002).
7. Tiziani H. J. and H.-M. Uhde, "Three-dimensional image sensing by chromatic confocal microscopy," Appl. Opt. **33**, 1838–1843, (1994).
8. Tiziani H. J. and Achi R. and Krämer R. N., "Chromatic confocal microscopy with microlenses," J. Mod. Opt. **43**, 155–163, (1996).

#1935 - $15.00 US
Received December 12, 2002; Revised January 09, 2003

9. O. Albert and L. Sherman and G. Mourou and T. B. Norris and G. Vdovin, "Smart microscope:an adaptive optics learning system for aberration correction in multiphoton confocal microscopy," Opt. Lett. **25**, 52–54 (2000).

1. Introduction

For precision instruments, accurate and quantitative profilometory combined with vibration tolerance are needed. Confocal microscopes have been widely employed, since they satisfy these requirements[1]. However, a confocal microscope is by nature a point measurement system for high order spatially dimensional measurements, meaning that a corresponding dimensional scanning operation is needed to determine spatially higher dimensional structure. This kind of scanning operation causes long measurement time, and in some application fields, this would create problems.

To reduce the need for lateral scanning, several kinds of tandem confocal microscopes [2], *e.g.*, confocal microscopes with a Nipkow disk[3, 1], with a microlens array objective[4, 5], and combined versions with rotating microlens array objectives[6] have been investigated.

A confocal microscope using chromatic aberration[7, 8] has been also developed to avoid the need for axial scanning, which focuses on an object at different axial positions depending on wavelength. This chromatic confocal microscope determines the object height using this feature. Although this system does not scan its focus axially, it requires a color detector and a broadband light source; it is also necessary to take into account the spectral absorption properties of the sample to be measured. Furthermore, when the object to be measured itself is flashing, for example on-site pit-depth measurement of laser welding, one of our target application, the flash interferes the measurement, although, in the case of monochromatic confocal system, it can be separated from signal light by a monochromatic filter.

In this letter, we propose a non-mechanically-axial-scanning confocal microscope with a monochromatic light source. This microscope switches the shape of an adaptive mirror into three or more patterns, and controls the defocus in an object space. Confocal intensity values, not axial responses, for each mirror shape are acquired, and the axial height of the object to be measured is determined according to these values.

2. Optical setup

Figure 1 shows the scheme for this confocal microscope. A 632.8 nm wavelength He-Ne laser is employed as a light source. The laser beam is expanded and collimated by lenses and a pinhole, then reflected by an electric field-driven membrane-adaptive mirror. The reflected beam is focused and reflected on the object surface through a polarization beam splitter (PBS), then re-reflected by the adaptive mirror. Finally the beam passes through a lens, L3, and forms a confocal spot on a CCD camera. Although conventional confocal microscopes use a pinhole and point-detector, in this setup we use a CCD, since we use the lateral profile of the confocal spot to optimize the shape of the adaptive mirror, as described below. This optimization is required only once for a new adaptive mirror, so that, in principle, we can replace the CCD with a conventional pinhole and a point detector after optimization to simplify the setup and to achieve more rapid measurement. The adaptive mirror carries out arbitrary defocus, allowing us to use it to axially scan the object. However, this system does not actually carry out the scanning operation by this means: it only switches the mirror shape into three to five patterns. The piezo-scanning stage on which the object to be measured is placed is driven only during initial calibration. It is never driven when taking actual measurements of itself. The beam is reflected by the adaptive mirror twice, meaning that, after the second

#1935 - $15.00 US Received December 12, 2002; Revised January 09, 2003

reflection, the wave front should be flat when the object surface is in focus.

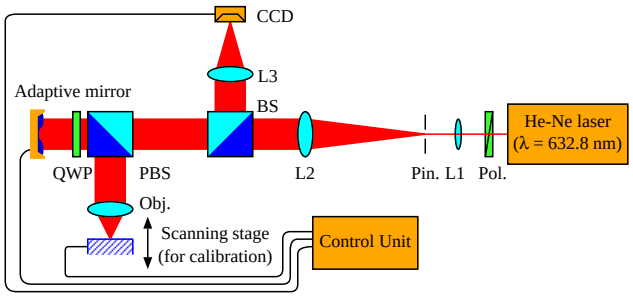

Fig. 1. The scheme of the developed confocal microscope. Pol. and QWP represent the polarizer and quarter wavelength plate, Pin. is the pinhole, BS and PBS are a beam splitter and a polarization beam splitter, Ls and Obj. are lenses and a microscope-objective, respectively. The scanning stage is a piezo-stage, which is driven only during initial calibration.

3. Optimization of adaptive mirror shape

This system switches the shape of the adaptive mirror and takes the confocal intensity output, not the axial response for each. Each mirror shape has a different defocus, making it possible to determine the height of the object from the resultant confocal intensities. A genetic algorithm is employed to optimize the mirror shape obtaining an arbitrary defocus. During the optimization process, a reference mirror is placed on the scanning stage, and its height is changed into 5 states in the range of $\pm$ 25 μm . The mirror shape is then optimized to focus on the surface of the reference mirror. Here, each optimized state is called a channel.

In the case of multi-photon or fluorescent confocal microscopes, confocal output intensity itself has been employed to characterize the degree of optimization as a cost function[9]. In the linear case, in a single-photon confocal microscope, this cost function not always work successfully, since it sometimes intensifies spherical aberration. We employed the spectral information entropy of the lateral confocal spot as a cost function. This spectral information entropy is introduced as follows. First, the discrete Fourier transform, $\hat{f}(\mu,\nu)$ of the confocal spot, $f(x,y)$ is calculated. The confocal spot itself is taken by the CCD camera. We then normalize the Fourier spectrum, and obtain the probability distribution of the spectrum as

$$P(\mu,\nu) = \frac{|\hat{f}(\mu,\nu)|}{\sum_{\mu,\nu}|\hat{f}(\mu,\nu)|}. \tag{1}$$

The information entropy is calculated from this probability distribution, as

$$\epsilon = -\sum_{\mu,\nu} P(\mu,\nu)\log P(\mu,\nu). \tag{2}$$

The genetic algorithm optimizes the mirror shape to maximize this information entropy. The information entropy decreases with the unevenness of the distribution $P(\mu,\nu)$: namely, it has a maximum value when all of the probability of Fourier spectrum is concentrated into one point, and has minimum value when the probabilities of Fourier spectrum for all positions have the same value. Hence, maximization of the information entropy of spectrum creates a confocal spot, which is of course the inverse-Fourier transformation of the spectrum, which is concentrated into one point. Although it also

#1935 - $15.00 US
Received December 12, 2002; Revised January 09, 2003

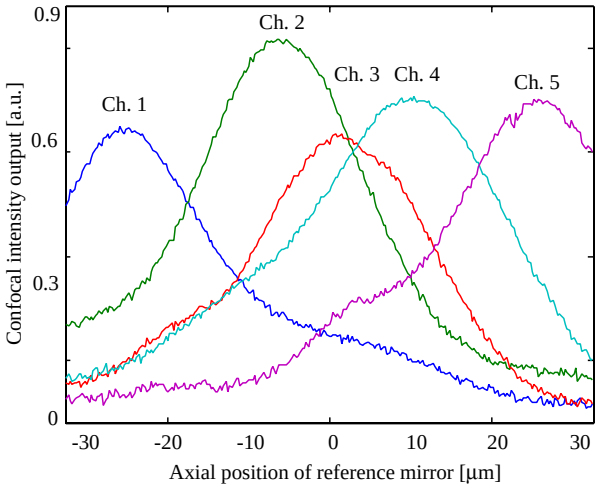

Fig. 2. Reference axial responses of each channel. Each channel is optimized with a different height of the reference mirror.

possible to optimize the mirror shape by minimizing the information entropy of the confocal spot itself, not its Fourier transform, in practice, this direct method sometimes does not work successfully. Because the confocal spot contains noise, and the adaptive mirror initially has defects, so that the initial spot shape sometime has two or more peaks, and it represents a local minimum of information entropy. In the spectral domain, these multiple peaks of the spot in the real domain insure interference fringes, and thanks to this effect, we can avoid generating this local minimum.

Each individual in the genetic algorithm holds the input voltages for each element of the adaptive mirror, 38 elements. There are 30 individuals in one generation. We evaluated 50 generations. In the evaluation process, each individual is ranked by their information entropy level as mentioned above, and parents for the next generation are picked randomly from the uppermost 75%. Then, randomly selected elements of the parents are randomly swapped with each other to generate individuals for the next generation. In this optimization process, the initial defects of the adaptive mirror are also canceled, removing the need for use of a high quality adaptive mirror.

4. Calibration

After optimization, the confocal axial responses for each channel are measured to calibrate the setup by means of axial scanning of the scanning stage. These axial responses will be used as reference channel outputs for the actual height measurement process. Here we used 2×2 pixels of a CCD camera, 22 μm $times$ 22 μm in size, although a pinhole and a point detector would be used in a conventional confocal microscope. Figure 2 shows the measured reference axial responses. Here we can see that the widths of the axial responses are larger than their theoretical value, although it does not make serious problems for surface measurement. The incompleteness of the optimization of the adaptive mirror, the shape of the pinhole, namely, square shape, not circular shape, and axial alignment error of the Fourier transform lens might make the axial response broaden.

#1935 - $15.00 US
Received December 12, 2002; Revised January 09, 2003

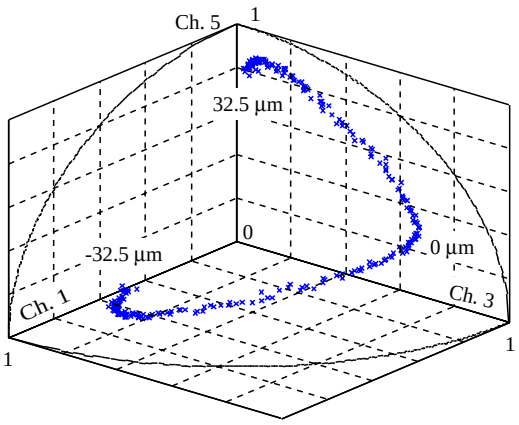

Fig. 3. Projection-plots of reference channel outputs. Each channel output is projected onto the surface of the unit sphere surface in the channel space, where each axis represents each channel.

5. Measurement and analysis process

In the actual height measurement process, axial scanning and axial confocal response are never acquired. Instead, we take only the confocal output values for each channel. These values are compared with the reference channel outputs which have been acquired during the calibration process to determine the height of the object. The actual procedure for converting the channel output values into height is follows. First, we assume a channel space where each axis represents an individual channel output, and project every reference output onto a unit spherical surface in this space. The coordinate vector on the surface of each reference output $\mathbf{r} = (r_1, r_2, \cdots)$ is expressed as

$$\mathbf{r} = \frac{\mathbf{R}}{|\mathbf{R}|} \tag{3}$$

where vector $\mathbf{R} = (R_1, R_2, \cdots)$ is a set of reference channel outputs which has been measured in the calibration process. A projection plot with 3 channels, channel 1, 3, and 5 in Fig. 2, is shown in Fig. 3. Here, the two end points of the plot represent the two end points of the measurement range, and their three turning points represent each maximum position of the reference axial responses. To determine the measured object height, the channel output values of the object measurement are also projected onto the same surface. Then the distance θ between this projection point and each reference point is calculated as

$$\theta = \arccos(\mathbf{r} \cdot \mathbf{m}) \tag{4}$$

where vector $\mathbf{m} = (m_1, m_2, \cdots)$ is the coordinate vector of the projection of measurement output. Finally, the closest neighboring reference point is sought, and the height of the reference point is regarded as the height of the measured object. To obtain practical accuracy, at least three channels are required. It means that this system can determine the height of an object using a three-shot measurement. It is clearly possible to use more channels and improve the accuracy and range of measurement, giving a trade-off between measurement time and accuracy or range. A five-channel version should have higher accuracy and a wider measurement range than a three-channel version. This was confirmed experimentally as described below.

#1935 - $15.00 US
Received December 12, 2002; Revised January 09, 2003

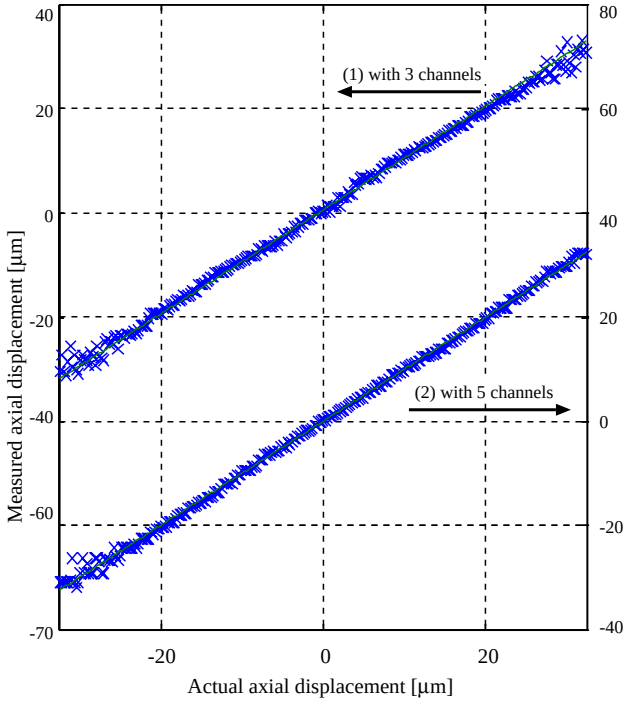

Fig. 4. Measured height of the object. The horizontal axial represents actual object height and the vertical axis represents measured height. Plots (1) and (2), respectively, are calculated from 3 and 5 channel-outputs. The solid lines represent theoretical lines.

6. Experimental demonstration

We measured several mirror heights using our prototype system to confirm the actual performance of this system. The axial height of the mirror was set at several different positions using a piezo-actuator. Figure 4 shows the measured height. The horizontal and vertical axes of this Figure, respectively, represent the displacement of the piezo-actuator, namely the actual height of the mirror, and the measured height; the solid lines represent theoretical lines. Plot (1) in Fig. 4 represents the results from a three-channel version using channels 1, 3 and 5 as shown in Fig. 2, and plot (2) depicts the results of using the five-channel version. The root mean square (RMS) errors from the theoretical lines in the 40 μm range are 0.48 μm for the three-channel version and 0.28 μm for the five-channel version. They are respectively 1.2% and 0.70% of the measurement range. It is also clear that the measurement range of the five-channel version is wider than that of the three-channel version, and further extension of measurement range is also available by using more channels. The RMS error of the five-channel version in the 50 μm range is 0.32 μm , equivalent to 0.64% of the range. These results suggest that the accuracy and measurement range of this system can be enhanced by using more channels.

7. Discussion

The lateral resolution of this system respects the numerical aperture (NA) of the objective and the wavelength of the light source. Here we use a 632.8 nm wavelength light source and objective of 140 mmNA = 0.25, so that the in-focus Rayleigh lateral resolution should be 1.54 μm . However, this system does not always operate in focus, since

#1935 - $15.00 US
Received December 12, 2002; Revised January 09, 2003

it determines axial height without scanning. The result is that the lateral resolution should be lower at the end of the measurement range than in the focal plane. In our prototype, lateral resolution with a 40 μm range is estimated to be 5 μm . On the one hand, the in-focus lateral resolution can be improved by using higher-NA objectives; on the other, such objectives make the focal depth shorter, resulting in a loss of out-of-focus resolution. Clearly, an objective with suitable NA should be selected to match the required resolution and measurement range.

The measurement time of this system is proportional to the response time of the adaptive mirror. The response time of the adaptive mirror employed here is 2 ms, so that the measurement time for one detection is 2 ms $\times$ the number of channels. Even for three-dimensional measurement, the number of channel switching is the same as with one-dimensional measurement, because once we switch the channel, it is fixed during lateral scanning. Hence the measurement time for three-dimensional measurement is chiefly restricted by lateral scanning time. Even in a highly dimensional case, we note that axial scanning is not required, and the measurement time is faster than achieved by conventional axial scanning methods.

Although our prototype system requires approximately 30 minutes for the optimization process using the genetic algorithm, most of this time is taken up with calculation of spectral information entropy. In this experiment we used a 90 MHz Pentium computer. Hence it should be easy to reduce the optimization time to several minutes by using a faster CPU. Furthermore, this optimization is needed only once for each new adaptive mirror, so that this optimization time is sufficiently short. This system takes approximately 5 minutes to obtain reference axial responses for each channel. In this case, too, most of the time is spent in computational operations, e.g., storing spot images. Since the calibration process is needed once a day or even less frequently, it should not cause a problem.

The two-dimensional imaging feature of a CCD camera is employed only during the optimization process. Optimization is in principle required only once for a new adaptive mirror. This means that once optimization is complete, we can replace the CCD camera with a conventional pinhole-point detector pair. The initial distortion of the adaptive mirror is also corrected by optimization, so that we can dispense with the need for an accurate and high quality adaptive mirror, and thus allowing this system to be built at relatively low cost.

8. Conclusion

We have developed a non-depth-scanning confocal microscope containing an adaptive mirror. This confocal microscope switches the shape of the adaptive mirror into three to five patterns. This system determines the height of an object without the need for axial scanning by using the confocal output values from each shape of the adaptive mirror. In some applications, for example on-site pit-depth measurement of laser welding; one of our target application, what we can avoid axial stage scanning makes some advantages, because the stage should be fixed in this kind of on-site measurement. Our prototype system has successfully determined the axial mirror position over a 50 μm range with a low 0.64% RMS error.

#1935 - $15.00 US Received December 12, 2002; Revised January 09, 2003